

Lawrence Berkeley National Laboratory

LBL Publications

Title

Sparse panicle1 is required for inflorescence development in *Setaria viridis* and maize

Permalink

<https://escholarship.org/uc/item/8j87h42p>

Journal

Nature Plants, 3(5)

ISSN

2055-026X

Authors

Huang, Pu

Jiang, Hui

Zhu, Chuanmei

et al.

Publication Date

2017

DOI

10.1038/nplants.2017.54

Peer reviewed

1 *Article type:* Letter

2

3 *Title: **sparse panicle1** is required for inflorescence development in *Setaria viridis* and maize*

4

5

6 *Author affiliations: **Pu Huang^{a,+}, Hui Jiang^{a,+}, Chuanmei Zhu^a, Kerrie Barry^b, Jerry Jenkins^c, Laura***
7 ***Sandor^b, Jeremy Schmutz^{b,c}, Mathew S. Box^a, Elizabeth A. Kellogg^a, Thomas P. Brutnell^{a,*}***

8

9 ^a Donald Danforth Plant Science Center, 975 N Warson Rd, St. Louis, MO 63132, USA

10 ^b Department of Energy Joint Genome Institute, Walnut Creek, California, USA

11 ^c HudsonAlpha Institute for Biotechnology, Huntsville, Alabama, USA

12 ⁺ These authors contributed equally to this work

13

14 ^{*} *Corresponding author:*

15 **Thomas P. Brutnell**

16 Donald Danforth Plant Science Center, 975 N Warson Rd, St. Louis, MO 63132, USA.

17 Tel: 1-314-587-1485

18 Email: tbrutnell@danforthcenter.org

19

20

21

22

23
24
25
26
27
28
29
30
31
32
33
34
35
36
37
38
39
40

Abstract

Setaria viridis is a rapid life cycle model panicoid grass^{1,2}. To identify genes that may contribute to inflorescence architecture and thus have the potential to influence grain yield in related crops such as maize, we conducted an NMU mutagenesis of *S. viridis* and screened for visible inflorescence mutant phenotypes³. Of the approximately 2700 M2 families screened we identified four recessive sparse panicle mutants (*spp1-spp4*) characterized by reduced and uneven branching of the inflorescence. To identify the gene underlying the *sparse panicle1* (*spp1*) phenotype, we performed bulked segregant analysis⁴ and deep sequencing to fine map it to an approximately 1 Mb interval. Within this interval we identified disruptive mutations in two genes. Complementation tests between *spp1* and *spp3* revealed they were allelic, and deep sequencing of *spp3* identified an independent disruptive mutation in *SvAUX1*, one of the two genes in the ~1Mb interval and the only gene disruption shared between *spp1* and *spp3*. *SvAUX1* was found to affect both inflorescence development and root gravitropism in *S. viridis*. A search for orthologous mutant alleles in maize confirmed a very similar role of *ZmAUX1* in maize, which highlights the utility of *S. viridis* in accelerating functional genomic studies in maize.

41
42 Maize (*Zea mays*) is one of the most important crop species globally, and has been used as a
43 genetic system since the early 20th century⁵. Two important goals of maize genetics are to define the
44 mode of action of genes that underlie agronomically important traits and to identify allelic variation that
45 can be exploited in maize breeding programs. Today, emerging food and energy crises demand rapid crop
46 improvement⁶, which will require the manipulation of genes underlying important traits. However, the
47 pace of gene discovery in maize is limited by the same traits that make it such a productive crop, namely
48 large stature, complex genome and long life span. Typical forward genetics studies in maize take years
49 from trait discovery to fine mapping of an underlying gene. To date, about 500 genes have been
50 characterized through genetic analysis over decades of study⁷. This contrasts sharply to thousands of
51 genes characterized in *Arabidopsis thaliana*, a rapid cycling eudicot which only became broadly adopted
52 as a model system in the mid 1980s^{8,9}. Indeed, many classical inflorescence mutants in maize, such as
53 *barren stalk1*¹⁰ and *barren inflorescence2 (bif2)*¹¹ were defined decades before the underlying genes were
54 finally discovered. Although *A. thaliana* is a very successful genetic model, over 140 million years of
55 evolutionary divergence¹² separates the two species that are morphologically, physiologically, and
56 developmentally distinct. For agronomically important traits that do not exist in *A. thaliana*, such as
57 complex inflorescence architecture, C₄ photosynthesis and grain starch accumulation, a grass model is
58 preferred¹.

59 In recent years *Setaria viridis* has been proposed as a model for food and bioenergy panicoid
60 crops, including maize^{1,2}. The lifespan, plant stature and genome size of *S. viridis* are comparable to *A.*
61 *thaliana*. The extensive gene synteny¹³, similar architecture and common habitats that *Setaria* shares with
62 maize suggest its great potential as a translatable model. However, to date neither the utility of *S. viridis*
63 as a genetic model system nor the translatability of discoveries from *S. viridis* to maize have been
64 demonstrated experimentally. In this study, we constructed a mutant population resource for *S. viridis*,
65 and used a forward genetic screen to dissect inflorescence architecture, a complex trait directly related to
66 yield and harvestability in maize and other cereal crops^{14,15}. We identified two independent mutations in a
67 single gene, *SvAUX1*, as responsible for major disruptions in inflorescence branch development, which
68 led to sparse panicle (*spp*) phenotypes. We then used a reverse genetics approach to show that a loss-of-
69 function allele in *ZmAUX1*, the maize ortholog of *SvAUX1*, conditions a maize male inflorescence
70 phenotype very similar to *spp1*, namely a reduction in primary branch formation, and thus likely acts
71 through similar genetic mechanisms. Trait discovery to fine map to *SvAUX1* in *S. viridis* took seven
72 months, with greatly lower associated costs and plant growth requirements than an equivalent study
73 would have taken in maize. Importantly, the translatability to maize was readily observed by exploiting
74 the phenotypic similarity and extensive synteny of the two species.

75 An N-Nitroso-N-methylurea (NMU)-induced mutant population of ~20,000 families was created
76 using reference line A10.1³. In total we screened ~2700 mutant families at the M2 generation for
77 phenotypes of interest and identified 61 mutant families for direct sequencing to empirically determine
78 the nature and frequency of chemically induced mutations (Table S1). Most of the changes observed were
79 transition mutations (e.g. G to A single nucleotide polymorphisms (SNPs)) (Fig. S1a). We found a
80 median of 66 homozygous nonsynonymous mutations per mutant family (Fig. S1b). Given this estimation
81 and a Poisson approximation, we estimate that in this population at least 17 mutant alleles exist for 95%
82 of the genes in the genome (Fig. S1c). Thus the *S. viridis* mutant population is a saturated population that
83 can be used for efficient forward and reverse genetics, and multiple alleles of the same gene can be
84 mined.

85 In an initial screen of ~700 mutant families, we obtained the first allele of the sparse panicle
86 (*spp1*) phenotype (Fig. 1a, i). Defects in *spp1* mutant panicles were detected early in inflorescence
87 development (11 days after germination; A10.1 panicles emerge at approximately 21 days in a chamber
88 under short day condition), as many primary branch primordia failed to initiate, and those that did form
89 were of unequal size. These changes resulted in disrupted phyllotaxis and ultimately the *spp* phenotype
90 (Fig. 1c, d). Direct sequencing of pooled DNA samples from three M3 individuals of this mutant family
91 identified 51 homozygous nonsynonymous mutations (Table S2). We used bulked segregant analysis
92 (BSA) with deep sequencing to fine map the causal mutation^{4,16}. To determine the effect of pool size and
93 marker density on mapping resolution and examine the effect of mutant alleles in different genetic
94 backgrounds, five F2 DNA pools from three different crosses were sequenced (Table 1). In all three
95 crosses, F1 plants resembled the A10.1 phenotype (wild-type, WT), and F2 plants displayed a segregation
96 ratio of 3:1 between WT and *spp1* (Table 1). Thus, *spp1* is inferred to be a recessive allele of a single
97 gene. A region of approximately 1Mb near the end of Chromosome 5 showed high homozygosity in all
98 five pools (Fig. 2a; Fig. S2). We did not observe strong differences in mapping resolution in the five
99 pools (Fig. S2) at the same sequencing depth (approx. 30x coverage). Thus, we suggest using a pool size
100 of 30 individuals from a backcross to A10.1 and a sequencing depth of 30x coverage as starting
101 conditions for future mapping attempts. However, if the causal gene is in a region of low recombination,
102 additional individuals may be needed. In this 1Mb region, only two nonsynonymous mutations located in
103 two genes were identified (Table S2). One gene is a ROP interaction partner homolog with unknown
104 function, the other gene is *SvAUX1* (Sevir.5G392400). To validate and fine map the mutation, we
105 identified three other families with *spp* phenotypes in an additional screen of ~2000 mutant families.
106 Among them, *spp3* most closely resembles *spp1* (Fig. 1a). Direct sequencing of *spp3* identified 98
107 homozygous nonsynonymous mutations in the genome (Table S3). *SvAUX1*, one of the two candidate
108 genes identified in the BSA, is the only gene with a homozygous nonsynonymous mutation in both *spp1*
109 and *spp3* genome-wide (Table S2; Table S3). The F1 hybrid between *spp1* and *spp3* shows a *spp*
110 phenotype, demonstrating *spp1* and *spp3* are non-complementing (Fig. 1b). Phenotypically both *spp1* and
111 *spp3* show decreased plant height, reduced inflorescence branching and spikelet numbers, and increased
112 panicle length compared to A10.1 (Fig. 1i, j; Fig. S3a-c). Collectively, these data indicate that *spp1* and
113 *spp3* are independently mutagenized alleles of *SvAUX1* that condition a *spp* phenotype and will hereafter
114 be referred to as *spp1-1* and *spp1-3*, respectively.

115 A phylogenetic analysis was performed using the coding sequences of *SvAUX1*, its homologs in
116 other grass species and *A. thaliana* (Fig. 2f). A homolog of *SvAUX1* in *A. thaliana*, *AtAUX1*, is a
117 polytopic membrane protein, and loss-of-function alleles lead to defects in auxin transport^{17,18} and
118 agravitropic responses in roots¹⁹. Loss-of-function alleles of the rice ortholog of *SvAux1*, *OsaAUX1*, show
119 agravitropic root growth and defects in lateral root²⁰ and root hair development²¹. The *SvAUX1* protein is
120 predicted to have 10 or 11 transmembrane domains¹⁷ and likely is necessary for auxin influx^{17,18}. The
121 *spp1-1* allele has a premature stop codon (W450*) which truncates the C terminus of the protein (Fig. 2b,
122 d). The C terminus of *AtAUX1* is known to be crucial for its auxin transport function^{17,18}. The *spp1-3*
123 allele has a substitution of a charged amino acid for an uncharged one (G332R) in transmembrane domain
124 7 (Fig. 2b, d), which could lead to conformational changes. Thus, both *spp1-1* and *spp1-3* are likely to be
125 loss-of-function alleles. To test whether *SvAUX1* has a conserved function in root development, we
126 examined root development and gravitropism in *spp1-1* and *spp1-3*. In both mutants, clear agravitropism
127 was observed (Fig. 1e). In a further experiment we changed the direction of the gravity vector during
128 active root growth and agravitropic responses were observed in both primary and lateral roots. Unlike

129 *OsAUX1* which is important for lateral root development, lateral root number was not affected in *spp1-1*
130 mutants (Fig. 1f; Fig. S3d). *SvAUX1* expression is universal in many organs, but its expression in root
131 and panicle is relatively higher than in other organs (Fig. S4c). This corresponds with our observed
132 mutant phenotypes in inflorescence and roots. Through quantitative reverse transcription PCR in
133 emerging panicles of A10.1 and *spp1-1*, we further show that *SvAUX1* is expressed consistently at a lower
134 level in *spp1-1* relative to A10.1 in emerging panicles. Thus, *spp1-1* may encode a message that is both
135 subject to nonsense-mediated decay²² and generate a truncated protein product (Fig. 1g).

136 In maize, defects in auxin biosynthesis^{23,24}, transport^{11,25} and signaling²⁶ have been linked to
137 inflorescence architecture variation, including branching pattern changes. This includes defects in the
138 presumed regulator of auxin effluxer *ZmPIN1*^{27,28}. However, to date, the maize auxin influx carrier
139 *ZmAUX1* has not been characterized. In both *AtAUX1* and *OsAUX1* single knockout mutants, no obvious
140 inflorescence phenotype was reported. Only in the triple or quadruple mutant of *AtAUX1* and its three
141 other paralogs were changes of phyllotaxy in shoot and inflorescence meristem observed²⁹. Accordingly,
142 the identification of *SvAUX1* as a causal gene for *spp1* hints that auxin influx may regulate inflorescence
143 architecture in maize. Phylogenetic analysis shows *SvAUX1* was co-orthologous to all four homologs in
144 *A. thaliana*. This is in contrast to the *AUX1* homologs of *S. viridis* and maize where clear one-to-one
145 orthology is observed across the phylogeny (Fig. S4). This result highlights the complexity of distant
146 monocot-eudicot comparisons and the ease of using *S. viridis* as model for panicoid crops like maize. We
147 identified a single ortholog (*ZmAUX1*, GRMZM2G127949) of *SvAUX1* in maize through gene synteny¹³
148 and phylogenetic analysis (Fig. 2f, Fig. S4). To examine the potential function of *ZmAUX1*, a *mutator*-
149 tagged allele (*Zmaux1-0*) was obtained from the UniformMu project³⁰. The *mutator* insertion is predicted
150 to disrupt the splicing signal of the first intron, and thus is likely to be a loss-of-function allele similar to
151 *spp1-1* and *spp1-3* (Fig. 2c, e). The tassel of *Zmaux1-0* homozygotes shows a clear disrupted branching
152 pattern, similar to *spp1* mutants in *Setaria*. (Fig. 1h, k). We then backcrossed *Zmaux1-0* to W22 and
153 quantified phenotypes in self pollinated progeny (BC1F2). Homozygous mutant tassels have significantly
154 reduced branch number, spikelet number in the central spike and first primary branch length compared to
155 W22 homozygotes and heterozygotes (Fig. S3e, f, i-l). We also often observed tassel nodes with no
156 primary branches, and some primary branches with very few spikelets in *Zmaux1-0* (Fig. S5). Although
157 the female inflorescence in maize (ear) does not have branches comparable to the tassel or to *S. viridis*,
158 we observed a bald tip on ears in homozygous *Zmaux1-0* and fewer spikelets per row (Fig. S3g; Fig. S5).
159 The disruption of inflorescence development in *Zmaux1-0* is generally less severe than auxin synthesis
160 mutants *sparse inflorescence1* and *vanishing tassell*^{23,24}, and auxin transport mutants such as *bif2*¹¹.
161 *ZmAUX1* is expressed in many organs, including immature tassel and ear. Furthermore, at least three
162 other homologs are also expressed in these tissues, including immature inflorescences (Fig. S4d). These
163 observations indicate the potential redundancy of gene functions among *AUX1* homologs in maize, and
164 perhaps explains the weaker phenotypes. Also as expected, the *Zmaux1-0* plants displayed a clear
165 agravitropic root growth phenotype (Fig. 1g; Fig. S3h).

166 Collectively, these results present a compelling case study for gene discovery in maize guided by
167 the genetics of the model grass *S. viridis*. Despite decades of genetic analysis of maize inflorescence
168 development, *ZmAUX1* had not previously been linked to inflorescence architecture, likely because of its
169 subtle phenotype and the lack of clear orthology to *A.thaliana*. In rice, knock-outs of the *ZmAUX1*
170 ortholog *OsAUX1* were recently reported in two separate studies, but both studies lacked descriptions of
171 inflorescence phenotypes^{20,21}. This suggests potential functional redundancy of the *Aux1* paralogs in rice.
172 The close phylogenetic relationship of *S. viridis* to maize together with their many anatomical and

173 biochemical similarities suggests that translating phenotypes from *S. viridis* to maize will be
174 straightforward. Indeed, high throughput suppressor or enhancer screens conducted with the *S. viridis*
175 *spp1* mutant alleles in greenhouse settings would likely reveal additional components of the auxin influx
176 pathway that would have conserved functions in maize. Unlike maize, *S. viridis* enables rapid gene
177 discovery through forward genetic approaches such as BSA. The time, expense and spatial requirements
178 associated with genetic studies in *S. viridis* are approximately less than 1/3 of that in target panicoid crops
179 like maize, sorghum and switchgrass. Thus *S. viridis* opens the opportunity of gene discovery in panicoid
180 grasses to researchers without access to large field sites or greenhouses. Given the importance of panicoid
181 grasses to global food security and bioenergy production, broader adoption of *S. viridis* by plant scientists
182 throughout the world should rapidly accelerate the understanding of plant gene function and lead to the
183 identification of novel breeding targets to enhance grain yield and biomass production.

184

185

186

187

188

189 **References**

- 190 1. Brutnell, T. P., Bennetzen, J. L. & Vogel, J. P. *Brachypodium distachyon* and *Setaria*
191 *viridis* : model genetic systems for the grasses. *Annu. Rev. Plant Biol.* **66**, 465–485 (2015).
- 192 2. Brutnell, T. P. Model grasses hold key to crop improvement. *Nature Plants* **1**, 15062
193 (2015).
- 194 3. Jiang, H., Huang, P. & Brutnell, T. P. in *Genetics and Genomics of Setaria* (eds. Doust,
195 A. & Diao, X.) **19**, (Springer International Publishing, 2016).
- 196 4. Michelmore, R. W., Paran, I. & Kesseli, R. V. Identification of markers linked to disease-
197 resistance genes by bulked segregant analysis: a rapid method to detect markers in
198 specific genomic regions by using segregating populations. *Proc. Natl. Acad. Sci. U. S. A.*
199 **88**, 9828–9832 (1991).
- 200 5. Emerson, R. A. The inheritance of certain ‘abnormalities’ in maize. *J. Hered.* **8**, 385–399
201 (1912).
- 202 6. Ray, D. K., Mueller, N. D., West, P. C. & Foley, J. A. Yield trends are insufficient to
203 double global crop production by 2050. *PLoS One* **8**, e66428 (2013).
- 204 7. Schnable, J. C. & Freeling, M. Genes identified by visible mutant phenotypes show

205 increased bias toward one of two subgenomes of maize. *PLoS One* **6**, e17855 (2011).

206 8. Koornneef, M. & van der Veen, J. H. Induction and analysis of gibberellin sensitive
207 mutants in *Arabidopsis thaliana* (L.) heynh. *Theor. Appl. Genet.* **58**, 257–263 (1980).

208 9. Redei, G. P. *Arabidopsis* as a genetic tool. *Annu. Rev. Genet.* **9**, 111–127 (1975).

209 10. Gallavotti, A. *et al.* The role of *barren stalk1* in the architecture of maize. *Nature*
210 **432**, 630–635 (2004).

211 11. McSteen, P. *et al.* *barren inflorescence2* Encodes a co-ortholog of the *PINOID*
212 serine/threonine kinase and is required for organogenesis during inflorescence and
213 vegetative development in maize. *Plant Physiol.* **144**, 1000–1011 (2007).

214 12. Wolfe, K. H., Gouy, M., Yang, Y. W., Sharp, P. M. & Li, W. H. Date of the
215 monocot-dicot divergence estimated from chloroplast DNA sequence data. *Proc. Natl.*
216 *Acad. Sci. U. S. A.* **86**, 6201–6205 (1989).

217 13. Schnable, J. C., Freeling, M. & Lyons, E. Genome-wide analysis of syntenic gene
218 deletion in the grasses. *Genome Biol. Evol.* **4**, 265–277 (2012).

219 14. Kellogg, E. Floral displays: genetic control of grass inflorescences. *Curr. Opin.*
220 *Plant Biol.* **10**, 26–31 (2007).

221 15. Sreenivasulu, N. & Schnurbusch, T. A genetic playground for enhancing grain
222 number in cereals. *Trends Plant Sci.* **17**, 91–101 (2012).

223 16. Takagi, H. *et al.* MutMap accelerates breeding of a salt-tolerant rice cultivar. *Nat.*
224 *Biotechnol.* **33**, 445–449 (2015).

225 17. Swarup, R. *et al.* Structure-function analysis of the presumptive *Arabidopsis*
226 auxin permease *AUX1*. *Plant Cell* **16**, 3069–3083 (2004).

227 18. Yang, Y., Hammes, U. Z., Taylor, C. G., Schachtman, D. P. & Nielsen, E. High-
228 affinity auxin transport by the *AUX1* influx carrier protein. *Curr. Biol.* **16**, 1123–1127 (2006).

229 19. Bennett, M. J. *et al.* *Arabidopsis AUX1* gene: a permease-like regulator of root
230 gravitropism. *Science* **273**, 948–950 (1996).

- 231 20. Zhao, H. *et al.* *OsAUX1* controls lateral root initiation in rice (*Oryza sativa* L.).
232 *Plant Cell Environ.* **38**, 2208–2222 (2015).
- 233 21. Yu, C. *et al.* The auxin transporter, *OsAUX1*, is involved in primary root and root
234 hair elongation and in Cd stress responses in rice (*Oryza sativa* L.). *Plant J.* **83**, 818–830
235 (2015).
- 236 22. Baker, K. E. & Parker, R. Nonsense-mediated mRNA decay: terminating
237 erroneous gene expression. *Curr. Opin. Cell Biol.* **16**, 293–299 (2004).
- 238 23. Phillips, K. A. *et al.* *vanishing tassel2* encodes a grass-specific tryptophan
239 aminotransferase required for vegetative and reproductive development in maize. *Plant Cell*
240 **23**, 550–566 (2011).
- 241 24. Gallavotti, A. *et al.* *sparse inflorescence1* encodes a monocot-specific YUCCA-
242 like gene required for vegetative and reproductive development in maize. *Proc. Natl. Acad.*
243 *Sci. U. S. A.* **105**, 15196–15201 (2008).
- 244 25. Gallavotti, A., Yang, Y., Schmidt, R. J. & Jackson, D. The relationship between
245 auxin transport and maize branching. *Plant Physiol.* **147**, 1913–1923 (2008).
- 246 26. Skirpan, A., Andrea, S., Xianting, W. & Paula, M. Genetic and physical
247 interaction suggest that *BARREN STALK1* is a target of *BARREN INFLORESCENCE2* in
248 maize inflorescence development. *Plant J.* **55**, 787–797 (2008).
- 249 27. Barazesh, S. & McSteen, P. *Barren inflorescence1* functions in organogenesis
250 during vegetative and inflorescence development in maize. *Genetics* **179**, 389–401 (2008).
- 251 28. Skirpan, A. *et al.* *BARREN INFLORESCENCE2* interaction with *ZmPIN1a*
252 suggests a role in auxin transport during maize inflorescence development. *Plant Cell*
253 *Physiol.* **50**, 652–657 (2009).
- 254 29. Bainbridge, K. *et al.* Auxin influx carriers stabilize phyllotactic patterning. *Genes*
255 *Dev.* **22**, 810–823 (2008).

256 30. Settles, A. M. *et al.* Sequence-indexed mutations in maize using the UniformMu
257 transposon-tagging population. *BMC Genomics* **8**, 116 (2007).

258

259 **Online material and methods**

260 ***NMU-induced S.viridis mutant population***

261 Mutant M1 seeds were obtained after treating A10.1 seeds with NMU (20mM) for 2, 3 and 4
262 hours³. Each M1 plant was self-pollinated to generate a mutant family for screening. To empirically
263 determine mutation rates, DNA samples were extracted from 61 mutant families. For each family, young
264 leaf tissue of one to four M3 or higher generation selfed individuals were collected (Supplementary Table
265 S1). For each family, DNA samples were pooled and sequenced to 20-30X coverage at JGI. Plate-based
266 DNA library preparation for Illumina sequencing was performed on the PerkinElmer Sciclone NGS
267 robotic liquid handling system using Kapa Biosystems library preparation kit. The pool of libraries was
268 then prepared for sequencing on the Illumina HiSeq sequencing platform utilizing a TruSeq paired-end
269 cluster kit, v4, and Illumina's cBot instrument to generate a clustered flowcell for sequencing. Sequencing
270 of the flowcell was performed on the Illumina HiSeq2500 sequencer using HiSeq TruSeq SBS
271 sequencing kits, v4, following a 2x150 indexed run recipe.

272 All reads were mapped to the *S. viridis* reference genome A10.1 (phytozome v11,
273 <http://phytozome.jgi.doe.gov/>) using bwa-mem³¹. SNPs were called using GATK unified genotyper³². To
274 distinguish SNPs generated by mutagenesis from those caused by residual heterozygosity, only SNPs
275 with alternative alleles occurring in a single family were considered. Effects of SNPs were predicted
276 using snpEff³³. During SNP calling, we found a large number of SNP calls due to either residual
277 heterozygosity or mapping errors in highly repetitive regions. These SNPs will cause an overestimation of
278 the SNP frequency caused by mutagenesis. To provide a more accurate estimation of the mutation rate,
279 we assume, given a random distribution of mutations caused by NMU, that it is statistically impossible to
280 observe the same SNP more than twice in the 61 sequenced families, whereas for SNPs caused by
281 mapping errors or residual heterozygosity (error-prone SNPs), higher frequencies are expected.
282 Accordingly, we applied a frequency filter to extract NMU-induced SNPs from background. SNPs that
283 occurred in a single mutant family and no other families were considered for frequency calculations. We
284 also generated a list of all the error-prone SNPs that are likely due to mapping error or residual
285 heterozygosity for downstream mapping in this study, as well as future mapping efforts using this NMU
286 population (File S1). All sequencing data were deposited to NCBI-SRA (Table S1).

287

288 ***Direct sequencing and bulked segregant analysis of spp mutants***

289 *spp1-1* and *spp1-3* were sequenced directly as part of the panel of NMU mutants. For bulked
290 segregant analysis of *spp1-1*, three crosses were performed between M3 individuals and three different
291 lines: reference line A10.1, another mutant line NMU00290 and a diverse accession TB0155,
292 respectively. We obtained five F2 mutant pools of variable sample sizes (Table 1). A binomial test was
293 applied to examine the fit of mutant and wild-type individuals to a Mendelian ratio of 3:1. Read mapping
294 and SNP calling were conducted as described above. All known error-prone SNPs and SNPs with
295 extremely high coverage (more than 100) were removed from the analysis. The homozygosity frequency
296 of each SNP and a sliding window smooth curve of 10 adjacent SNPs were calculated. Sequences for the
297 five pools were processed separately first, then the resulting allele frequencies of all five pools were
298 merged. For the summarized analysis in order to make the results from different pools comparable, only
299 SNPs overlapping with direct sequencing results from *spp1* were considered.

300

301 ***Plant growth and histology***

302 All plants were grown in a growth chamber under short day conditions (31 °C/22 °C (day/night),
303 12 hr light/12 hr dark, 50% relative humidity) at the Donald Danforth Plant Science Center. For scanning
304 electron microscope (SEM) work, samples were fixed and dehydrated using standard protocols³⁴ and
305 critical point dried (CPD) using a Tousimis Samdri-780a. Images were taken with a Hitachi S2600 SEM
306 at Washington University's Central Institute for the Deaf. Input levels and brightness were adjusted in
307 Adobe Photoshop. For the root gravitropism assay, *S. viridis* seeds were sterilized with 20% bleach for 20
308 min and rinsed 5 times with sterile water. Seeds were kept in water at 4 °C for 3 days and then grown on
309 medium (0.5X Murashige and Skoog basal salt, 1% sucrose, 0.8% agar, pH=5.7). Plants were grown with
310 200 μmol/m²s of 12 hour light (6 am-6 pm) , 31 °C day/22 °C night temperature, 50% humidity. Maize
311 seeds were sterilized with 35% hydrogen peroxide for 20 min and rinsed 5 times with sterile water. Seeds
312 were incubated with water in the dark at 30°C for 2 days to germinate and then transferred to medium (1X
313 Hoagland's solution, 0.15% gelzan, pH=6). Plants were grown with 600 μmol/m²s, 18 hour light (6am-
314 10pm), 28 °C day/ 24 °C night temperature, 50% humidity.

315 Mutant family UFMU06246, which contains a mutator insertion in GRMZM2G127949 was
316 ordered from Maize Genetics Cooperation (maizecoop.cropsci.uiuc.edu/request/). We identified
317 homozygous individuals through a PCR assay with gene-specific and mutator-specific primers (Table
318 S4). The position of the mutator insertion was confirmed by Sanger sequencing. Seedling gravitropism
319 assays were performed with selfed progeny of these materials. Mutants were backcrossed to W22 and the
320 F1 plants self-pollinated to create a BC1F2 population. Individuals of the BC1F2 population were
321 genotyped using a PCR assay using the same primers that were used previously (Table S4). Plants were
322 propagated under normal greenhouse conditions (14 hour light, 26-28 °C day/22-24 °C night
323 temperature). All panicle and whole plant phenotypes were measured in the BC1F2 population.

324

325 ***Protein structure, phylogenetic and expression characterizations of SvAUX1 and ZmAUX1***

326 Protter³⁵ was used to predict transmembrane domains of *SvAUX1* and *ZmAUX1*. Homologs of
327 *SvAUX1* were identified using BLASTN³⁶ with default settings to primary CDS sequences of grasses and
328 *A. thaliana* (<http://phytozome.jgi.doe.gov/>). Sequences were aligned using MAFFT³⁷, and phylogenetic
329 analyses were performed using the maximum likelihood method and GTR+G+I model using RaxML³⁸. A
330 rapid bootstrap was performed 1000 times, and the consensus tree was built using the extended majority
331 rule of RaxML. *In silico* data of the expression levels of *SvAUX1* and *ZmAUX1* in *S. viridis* and maize
332 were obtained from the *S. viridis* gene atlas project (<http://phytozome.jgi.doe.gov/>) and maize gene
333 atlas³⁹, respectively.

334 For quantitative reverse transcription PCR, RNA was extracted from emergent panicles of A10.1
335 and *spp1*, each with three biological replicates. The RNA extraction followed the recommended protocol
336 of TriPure isolation reagent (Sigma-Aldrich). Reverse transcription was performed according to the
337 manufacturer's recommendation (Invitrogen SuperScript III first strand synthesis system), using polyT as
338 primers. To avoid inconsistencies of reference gene expression, we used two reference genes
339 *Sevir.9G574400*⁴⁰ and *Sevir.2G354200*⁴¹ for comparisons. The primers were designed to be intron-
340 spanning or intron junction spanning to avoid non-specific amplification of genomic DNA (Table S4).
341 Primer efficiencies were determined by a serial 50% dilution using a Roche 480 LightCycler system.
342 Quantitative PCR and data analysis were carried out using recommended settings of the Roche 480
343 LightCycler system and LightCycler 480 SYBR Green I Master. The normalized relative quantity to the
344 two reference genes was estimated using the method described in⁴².

345

346 ***Data availability***

347 All sequencing data can be accessed through NCBI-SRA. Detailed accession numbers were listed in
348 Table S1. All the error-prone SNPs from the NMU population that are likely due to mapping error or
349 residual heterozygosity were listed in File S1.

350

351

352

353

354

355

356

357

358

359

360 **Author Contributions**

361 P.H., H.J. and T.P.B. conceived and designed the study. H.J. performed the screen, crosses and DNA
362 extraction. P.H. and H.J. performed bulked segregant analysis. K.B., J.J., L.S. and J.S. performed library
363 construction and sequencing. P.H. performed sequencing and other data analysis. P.H., H.J., C.Z. and
364 M.S.B. performed phenotypic characterizations in *S. viridis* and maize. P.H., H.J., C.Z., E.A.K. and T.B.
365 wrote the manuscript.

366

367 **Acknowledgements**

368 The authors thank Dr. Adam Bray for his help in maize root gravitropism assay, Dr. Christine
369 Shyu for her help in qRT-PCR, and the DDPSC greenhouse staff for plant care. The work conducted by
370 the U.S. Department of Energy Joint Genome Institute was supported by the Office of Science of the US
371 Department of Energy under contract number DE-AC02-05CH11231. This work was also supported by a
372 Department of Energy grant to T. Brutnell (DE-SC0008769), and a National Science Foundation grant to
373 E. A. Kellogg (IOS-1413824).

374

375

376

377 Reference for online methods:
378

- 379 31. Li, H. Aligning sequence reads, clone sequences and assembly contigs with BWA-MEM.
380 *arXiv* **1303.3997**, (2013).
- 381 32. McKenna, A. *et al.* The Genome Analysis Toolkit: a MapReduce framework for analyzing
382 next-generation DNA sequencing data. *Genome Res.* **20**, 1297–1303 (2010).
- 383 33. Cingolani, P. *et al.* A program for annotating and predicting the effects of single nucleotide
384 polymorphisms, SnpEff: SNPs in the genome of *Drosophila melanogaster* strain w1118;
385 iso-2; iso-3. *Fly* **6**, 80–92 (2012).
- 386 34. Hodge, J. G. & Kellogg, E. A. Patterns of inflorescence development of three prairie
387 grasses (Andropogoneae, Poaceae). *Int. J. Plant Sci.* **175**, 963–974 (2014).
- 388 35. Omasits, U., Ahrens, C. H., Müller, S. & Wollscheid, B. Protter: interactive protein feature
389 visualization and integration with experimental proteomic data. *Bioinformatics* **30**, 884–886
390 (2014).
- 391 36. Altschul, S. F., Gish, W., Miller, W., Myers, E. W. & Lipman, D. J. Basic local alignment
392 search tool. *J. Mol. Biol.* **215**, 403–410 (1990).
- 393 37. Katoh, K., Misawa, K., Kuma, K.-I. & Miyata, T. MAFFT: a novel method for rapid multiple
394 sequence alignment based on fast Fourier transform. *Nucleic Acids Res.* **30**, 3059–3066
395 (2002).
- 396 38. Stamatakis, A. RAxML version 8: a tool for phylogenetic analysis and post-analysis of large
397 phylogenies. *Bioinformatics* **30**, 1312–1313 (2014).
- 398 39. Stelpflug, S. C. *et al.* An Expanded Maize Gene Expression Atlas based on RNA
399 Sequencing and its Use to Explore Root Development. *Plant Genome* **9**, 0 (2016).
- 400 40. Lambret-Frotté, J. *et al.* Validating Internal Control Genes for the Accurate Normalization of
401 qPCR Expression Analysis of the Novel Model Plant *Setaria viridis*. *PLoS One* **10**,
402 e0135006 (2015).

- 403 41. Dong, M. A., Farré, E. M. & Thomashow, M. F. Circadian clock-associated 1 and late
404 elongated hypocotyl regulate expression of the C-repeat binding factor (CBF) pathway in
405 *Arabidopsis*. *Proc. Natl. Acad. Sci. U. S. A.* **108**, 7241–7246 (2011).
- 406 42. Hellemans, J., Mortier, G., De Paepe, A., Speleman, F. & Vandesompele, J. qBase relative
407 quantification framework and software for management and automated analysis of real-time
408 quantitative PCR data. *Genome Biol.* **8**, R19 (2007).

409

410

411
412
413

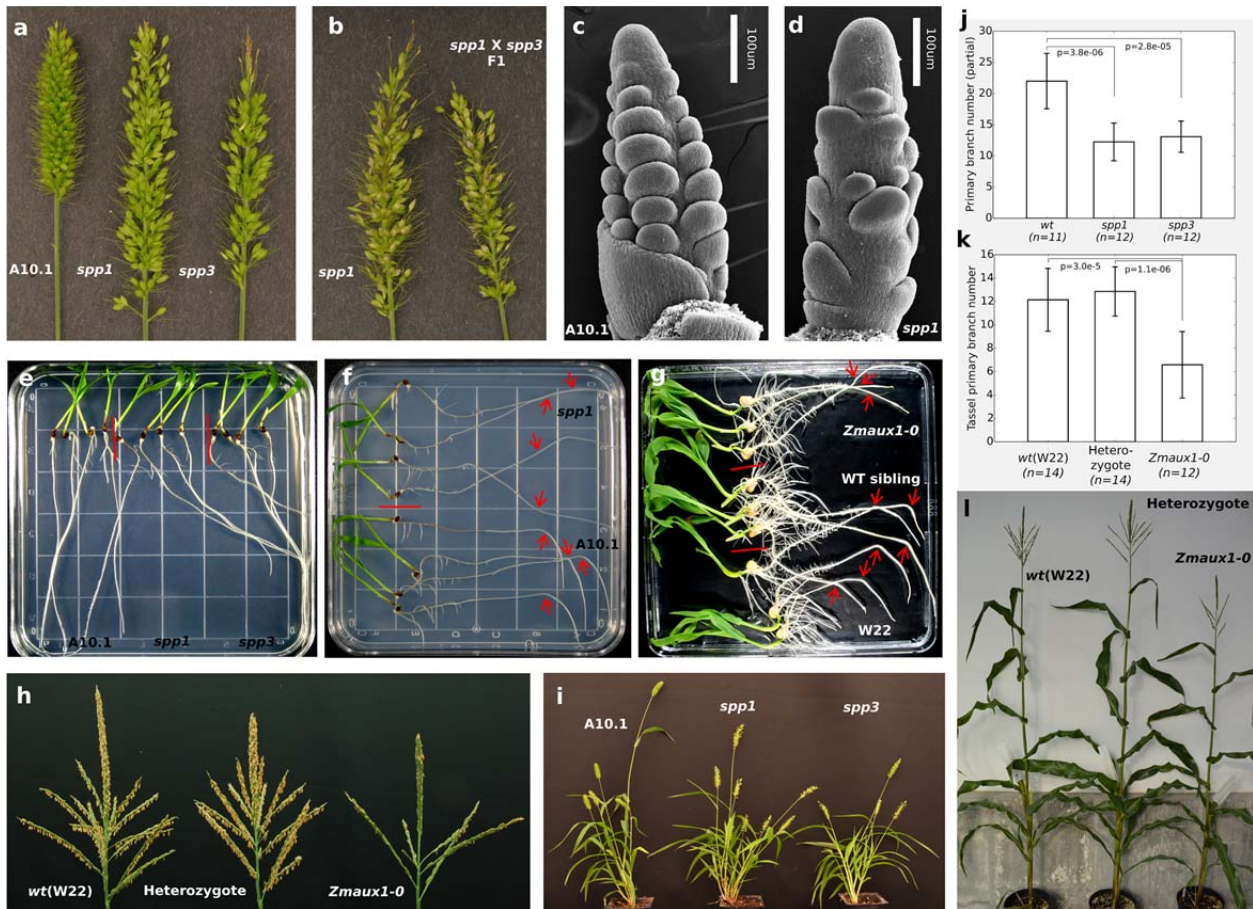
Table 1. Populations for bulked segregant analysis

Parent 1	Parent 2	Segregation WT: <i>spp1</i>	p ^a	No. of F2 individuals pooled	Median fold coverage (genome wide)
NMU00629.3m (<i>spp1-1</i>)	TB0155	147:45	0.54	44	29
NMU00629.3m (<i>spp1-1</i>)	NMU00290 ^b	304:105	0.67	30	24
				60	30
NMU00629.3m (<i>spp1-1</i>)	A10.1 ^b	272:94	0.70	30	30
				64	26

414
415
416
417

^a p value of two-tailed binomial test of expected ratio 3:1

^b two DNA pools of different sizes were made from mutants generated by each cross.

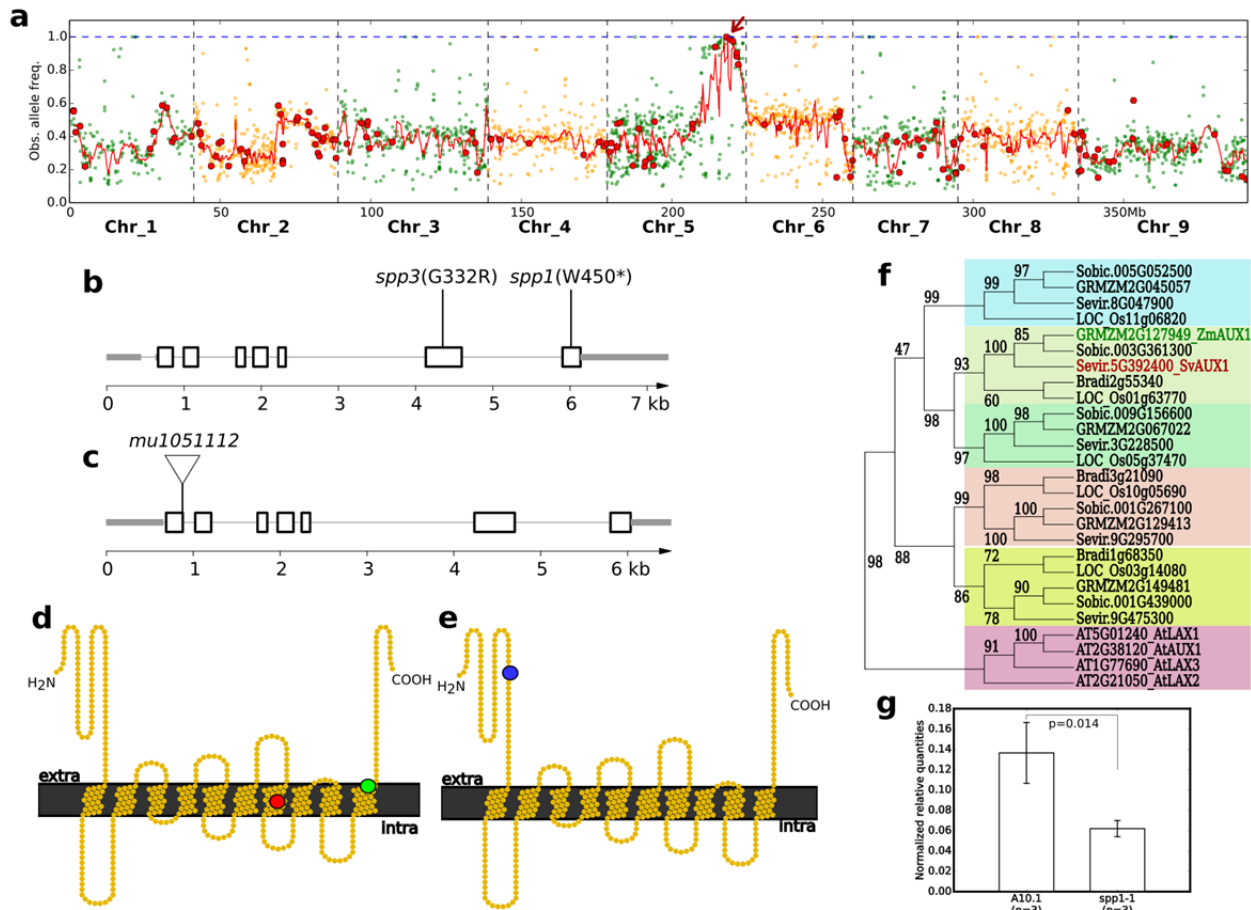


419 **Figure 1.** Characterization of *spp1* and *spp3* in *S. viridis* and *Zmaux1-0* in maize. **a)** Reduced branching
 420 of panicles in *spp1* and *spp3*. **b)** Complementation test between *spp1* and *spp3*; hybrid shows *spp*
 421 phenotype. **c,d)** Early panicle development (11 days after germination) of A10.1 and *spp1*. **e)** Root
 422 growth of A10.1, *spp1* and *spp3*, 6 days after germination. **f)** Root gravitropism assay for A10.1 and *spp1*.
 423 **g)** Root gravitropism assay for *Zmaux1-0*, segregating wild type siblings from the same mutant family
 424 and wild type background (W22). In F and G, the direction of the gravity vector was changed 90°
 425 clockwise at 4 days after germination, and the photo was taken at day 5 (*S. viridis*) or day 6 (maize). Red
 426 arrows indicate the positions of root tips at day 4 before rotating the plates. Seedlings of different
 427 genotypes are indicated by red vertical lines. **h)** Inflorescence phenotype of wild type (W22),
 428 heterozygote and homozygote of *Zmaux1-0*. **i)** Mature A10.1, *spp1* and *spp3* in *S. viridis*. **j)** Inflorescence
 429 primary branch number of A10.1, *spp1* and *spp3* in *S. viridis*, measured from bottom, 0.5 cm to 1.5 cm. **k)**
 430 Tassel primary branch number of WT, heterozygote and homozygous *Zmaux1-0*, from the bottom 5 cm.
 431 All bar heights show mean values, error bars show standard deviations, p-values were calculated from
 432 two-tailed t-tests and n= number of individuals examined. **l)** Mature plant of W22, heterozygote and
 433 *Zmaux1-0*.
 434

435

436

437
438
439
440



441
442
443
444
445
446
447
448
449
450
451
452
453
454
455
456
457

Figure 2. BSA mapping and variation of *SvAUX1* and *ZmAUX1* alleles. **a)** Bulked segregant mapping (BSA) of *spp1*, showing combined result from all five pools. The red arrow indicates the mutation in *SvAUX1* in *spp1*. **b)** Position of mutations in *SvAUX1* in *spp1* and *spp3*. **c)** Position of Mutator insertion in *ZmAUX1* in *Zmaux1-0*. **d)** Predicted transmembrane domains of *SvAUX1* protein. Red and green circles show amino acids affected by *spp1-1* and *spp1-3* mutations, respectively. **e)** Predicted transmembrane domains of *ZmAUX1* protein. Blue circle shows position of presumed protein truncation associated with *Mutator* insertion in *Zmaux1-0*. **f)** Phylogeny of *AUX1* homologs. This tree is a consensus tree of 1000 bootstraps using GTR+G+I model in RaxML. Red and green homologs denote *SvAUX1* and *ZmAUX1*, respectively. Node labels show bootstrap support percentage, and background highlight denotes five highly supported ortholog clades in grasses and one clade for homologs in *A. thaliana*. **g)** Normalized relative expression of *spp1-1* and A10.1 alleles of *SvAUX1* to reference genes *Sevir.2G354200* and *Sevir.9G574400* from qRT-PCR. Bar heights show mean values, error bars show standard deviations, p-values calculated from two-tailed t-test, and 3 biological replicates were made in both A10.1 and *spp1-1*.

